JOURNAL OF GEOPHYSICAL RESEARCH, VOL. 105, NO. B11, PAGES 25,955–25,968, NOVEMBER 10, 2000

The stability and P–V–T equation of state of $CaSiO_3$ perovskite in the Earth's lower mantle

Sang-Heon Shim and Thomas S. Duffy

Department of Geosciences, Princeton University, Princeton, New Jersey

Guoyin Shen

GeoSoilEnviro Consortium for Advanced Radiation Sources, University of Chicago
Chicago, Illinois

Abstract. Energy dispersive X-ray diffraction measurements for polycrystalline $CaSiO_3$ perovskite were carried out at in situ transition zone and lower mantle P–T conditions (P=18–96 GPa, T=1238–2419 K) using the diamond anvil cell and double-sided laser heating at the GeoSoilEnviro Consortium for Advanced Radiation Sources (GSECARS) sector of the Advanced Photon Source. An analysis of the temperature error sources in laser heating reveals that the axial and radial thermal gradients are the greatest error source. We have used measurements where the combined temperature error (1σ) from all sources is <150 K. By obtaining X-ray diffraction patterns at 8–22 GPa and 300–2200 K range, the high-temperature phase boundary between $CaSi_2O_5$+Ca_2SiO_4 and $CaSiO_3$ perovskite was determined to be 14–16 GPa, in contrast to the results of previous large-volume press (LVP) measurements (9–11 GPa). The stability of cubic $CaSiO_3$ perovskite was confirmed to 2300 km depth in the Earth's interior. No evidence of phase transformation or break down to oxides was observed. The proposed tetragonal distortion, and hence the phase transformation from distorted phase to cubic, was not observed. The combined data set of this study and earlier LVP measurements was fit to a Birch-Murnaghan-Debye equation. By fixing $V_0 = 27.45$ cm^3/mol, $K_{T0} = 236$ GPa, and $K'_{T0} = 3.9$ from recent static compression data and $\theta_0 = 1000$ K, we obtain $\gamma_0 = 1.92 \pm 0.5$ and $q = 0.6 \pm 0.3$. Although data to 69 GPa and 2380 K were used in the fitting, this result is also consistent with measurements to 96 GPa. This result yields not only density and bulk modulus but also higher-order thermoelastic parameters, such as thermal expansivity and temperature dependence of bulk modulus, at lower mantle P–T condition in an internally consistent way. This direct measurement of the equation of state at lower mantle condition verifies that the density and bulk modulus of $CaSiO_3$ perovskite at lower mantle P–T conditions are very close to seismic values (within 1.5 and 3.0%, respectively). These differences are sufficiently small that the abundance of $CaSiO_3$ perovskite will have negligible effects on density and bulk modulus profiles for the mantle.

1. Introduction

The physical properties and the phase transformations of calcium-bearing phases are important for understanding the dynamics and the evolution of the mantle [*Ringwood,* 1975; *Duffy and Anderson,* 1989]. In the transition zone, calcium is largely incorporated into the garnet phase and transforms between 580 and 720 km depth into $CaSiO_3$ in the perovskite structure [*Mao et al.,* 1977; *Tamai and Yagi,* 1989; *Oguri et al.,* 1997; *Hirose et al.,* 1999].

There have been few detailed studies about the phase relationships in the CaO-SiO_2 system at transition zone conditions [e.g., *Gasparik et al.,* 1994; *Wang and Weidner,* 1994]. The stability and the physical properties of $CaSiO_3$ perovskite have not previously been examined directly at lower mantle P–T conditions. The stability at lower mantle pressures were confirmed only at 300 K [*Tamai and Yagi,* 1989; *Yagi et al.,* 1989; *Tarrida and Richet,* 1989; *Mao et al.,* 1989]. The P–V–T equation of state (EOS) was measured using a large-volume press (LVP) [*Wang and Weidner* 1994; *Wang et al.,* 1996]. However, this measurement was performed

Copyright 2000 by the American Geophysical Union.

Paper number 2000JB900183.
0148-0227/00/2000JB900183$09.00

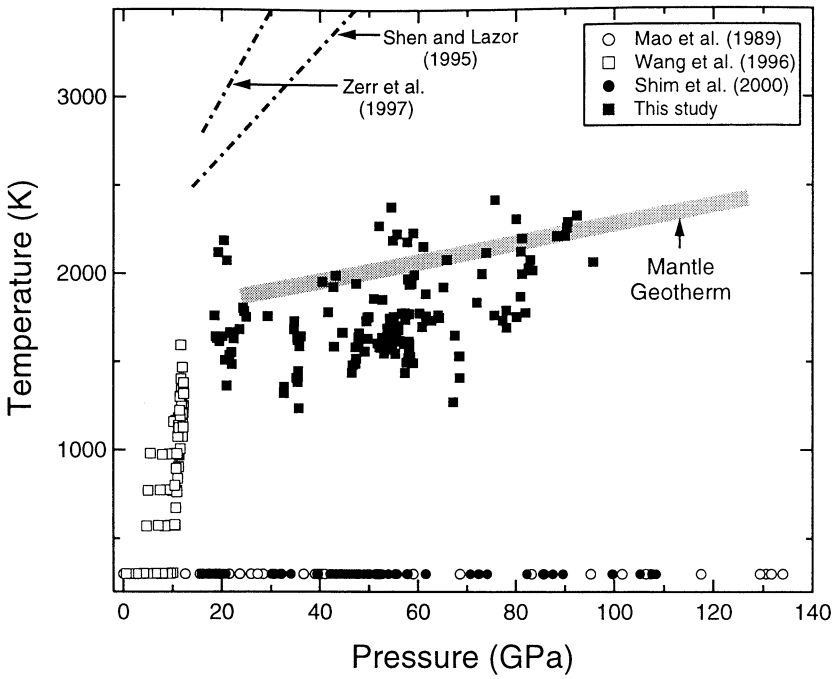

Figure 1. P–T conditions of this study for $CaSiO_3$ perovskite. Those of other studies [*Mao et al.*, 1989; *Wang et al.*, 1996; *Shim et al.*, 2000] are also plotted for comparison. Mantle P–T conditions are from the Preliminary Reference Earth Model (PREM) [*Dziewonski and Anderson*, 1981] and *Brown and Shankland* [1981]. Melting curves of $CaSiO_3$ perovskite (dash-dotted lines) are from *Shen and Lazor* [1995] and *Zerr et al.* [1997].

at low P–T conditions ($P < 12$ GPa and $T = 300$–1600 K) and requires long extrapolation to derive physical properties, such as density and bulk modulus, at lower mantle conditions.

Recent new developments in the laser heating techniques with the diamond anvil cell (DAC) enable us to explore the stability and the physical property of materials directly at the Earth's deep interior conditions [*Boehler et al.*, 1990; *Shen et al.*, 1996; *Boehler*, 1996; *Shen et al.*, 1998; *Fiquet et al.*, 2000; *Dewaele et al.*, 2000]. The improvement in temperature homogeneity in the heated area opens new opportunity to measure the P–V–T relationship at extreme P–T conditions [*Shim et al.*, 1998; *Fiquet et al.*, 1998, 2000; *Dewaele et al.*, 2000; *Shen et al.*, 2000]. *Shim and Duffy* [2000] showed that P–V–T measurements using the laser-heated diamond anvil cell (LHDAC) have the potential to provide not only direct measurements of density and bulk modulus at lower mantle conditions but also to resolve higher-order thermoelastic parameters, such as the volume dependence of Grüneisen parameter, temperature derivative of bulk modulus. However, they also demonstrated that temperature inhomogeneity could result in systematic error in fitted parameters. This indicates that the identification of the error sources in laser heating and their effects on EOS fitting is crucial to pursue P–V–T measurements and for making further technical improvement in laser heating. Here we report P–V–T measurements on $CaSiO_3$ perovskite at 18–96 GPa and 1238–2419 K, corresponding to the Earth's transition zone and most of the lower mantle (Figure 1).

2. Experimental Techniques

2.1. Sample Preparation

A natural wollastonite from Newburg, New York, was used as the starting material. X-ray diffraction and scanning electron microscope analysis of the starting material confirmed that is a pure phase with only negligible amounts (<0.1 mol %) of Fe and Mn impurities. The wollastonite powder was mixed with 10 wt % platinum powder, which was used as a laser beam absorber and pressure standard using the EOS of *Holmes et al.* [1989].

A thin (10 μm) foil of the wollastonite-platinum mixture was loaded in a preindented stainless steel gasket with a 150-μm-diameter hole and compressed using 300-μm diamond anvils for experiments covering 10–70 GPa. For higher pressures we loaded the foil in a 50-μm hole in a rhenium gasket. Beveled diamond anvils with 100-μm central flats were used in this case. A pressure medium and insulation layer of either NaCl or argon was loaded together with the sample foil in such a way that the sample foil was not in direct contact with the diamond anvils.

2.2. X-Ray Diffraction

Energy dispersive X-ray diffraction (XRD) measurements were carried out using a tapered undulator source at the GeoSoilEnviro Consortium for Advanced Radiation Sources (GSECARS) sector of the Advanced Photon Source [*Rivers et al.*, 1998]. A 10 μm×10 μm X-ray beam was used. This small beam size is important to collect the XRD spectra from an area with a homogeneous temperature distribution, since the flat top of the temperature profile is typically 20 μm in diameter.

For $CaSiO_3$ perovskite, at least three diffraction lines were readily observed to 96 GPa and 2419 K (Figure 2) and used for unit cell calculation. In most cases, two diffraction lines were observed for platinum. However, at 85–96 GPa the 111 and 200 platinum peaks are overlapped by argon lines. Except in this region, at least two lines of platinum were used to calculate its unit cell parameters.

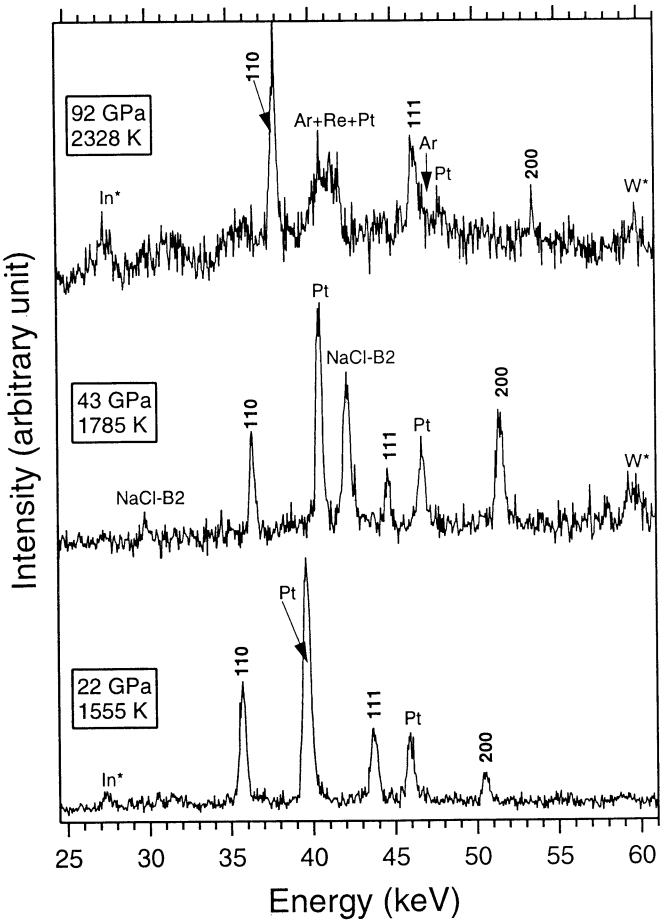

Figure 2. X-ray diffraction patterns of $CaSiO_3$ and platinum at lower mantle P–T conditions. The $CaSiO_3$ diffraction lines are indexed. NaCl or argon was used as a pressure transmitting and insulation medium. B2 refers to the high-pressure phase of NaCl. The fluorescence lines of indium and tungsten (indicated by asterisk) arise from laser and X-ray optics.

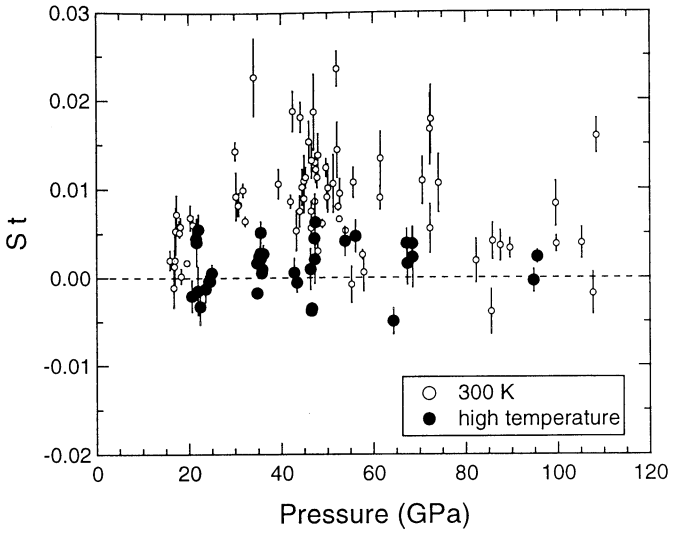

Figure 3. Product of elastic anisotropy and uniaxial stress component St for $CaSiO_3$ perovskite at both high temperature and 300 K [*Shim et al.*, 2000]. The estimated error is 1σ. The high temperature data points shown correspond to the points in Table 1.

According to lattice strain theory [*Singh*, 1993; *Duffy et al.*, 1999; *Shim et al.*, 2000], relative shifts of individual diffraction lines for a sample under non hydrostatic stress can be described by the differential stress t, elastic anisotropy S, and the angle ψ, between the diamond cell stress axis and the normal to the diffracting planes:

$$\frac{a(hkl) - a(hkl^*)}{a_0} = -St(1-3\cos^2\psi)[\Gamma(hkl)-\Gamma(hkl^*)], \quad (1)$$

where $a(hkl)$ is the calculated unit-cell parameter from a single diffraction line, and the asterisk denotes a reference diffraction line (in this study the 200 line is used as a reference for both $CaSiO_3$ perovskite and platinum) and the subscript zero denotes ambient conditions. The differential stress or uniaxial stress component t is the difference between the principal stresses in the axial and radial directions of the diamond anvil cell. $\Gamma(hkl)$ is given by

$$\Gamma(hkl) = \frac{h^2k^2 + k^2l^2 + l^2h^2}{(h^2 + k^2 + l^2)^2}, \quad (2)$$

where hkl are the Miller indices of an individual diffraction line. The slope of a linear fit of the diffraction data to Equation (1) yields a parameter that is the product of the elastic anisotropy S and the uniaxial stress component t. The details of the methodology are described elsewhere [*Shim et al.*, 2000].

The product St obtained from this fit can be used as an indicator of the stress condition of the sample. At a given pressure and temperature a larger St value indicates a larger uniaxial stress component t since S

is constant. Heterogeneous stress conditions induce a range of St values at a given pressure as has been found by *Shim et al.* [2000] for temperature-quenched $CaSiO_3$ perovskite samples. In this interpretation, the scatter of previous static compression data points from different experiments at 300 K was explained by variations in deviatoric stress conditions. In order to obtain an accurate P–V EOS, *Shim et al.* [2000] selected data points with low St values ($|St| \leq 0.005$).

The St value of $CaSiO_3$ perovskite at high temperature is always within the range of $-0.005 \sim 0.005$ (Figure 3). In contrast to the 300 K case where the average St value is +0.012 over the measured pressure range, the St at high temperature has an average value of 0. In addition, during heating, a 20–30% decrease of peak width is readily observed for both $CaSiO_3$ perovskite and platinum. These indicate that while significant deviatoric stresses in $CaSiO_3$ perovskite may exist at room temperature, the stress state at high temperature is more hydrostatic.

2.3. Laser Heating

Two Nd:YLF laser beams were used to simultaneously heat the sample on both sides. This technique has been described in detail elsewhere [*Shen et al.*, 2000]. The temperature is also measured on both sides independently (Figure 4). This design reduces the thermal gradient along the loading axis of the DAC significantly. To decrease the thermal gradient along the radial direction, a TEM_{01} (TEM: transverse electromagnetic, TEM_{01}: donut shaped mode) laser mode is used to provide a large (20–30 μm) flat-topped temperature profile. The temperature profile across the heated area is measured using a charge-couple device with a spatial resolution of 1.7 μm (Figure 5).

Before each heating run we carefully aligned the laser beams to the center of the X-ray position (which is visible due to X-ray fluorescence) using a video monitoring system. The intensity of this diamond fluorescence is 10^3–10^4 times weaker than the thermal radiation.

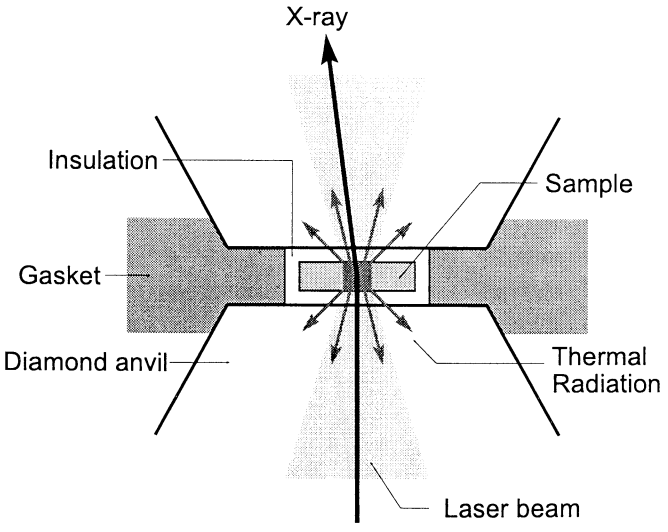

Figure 4. Schematic diagram of double-sided laser-heated diamond cell geometry.

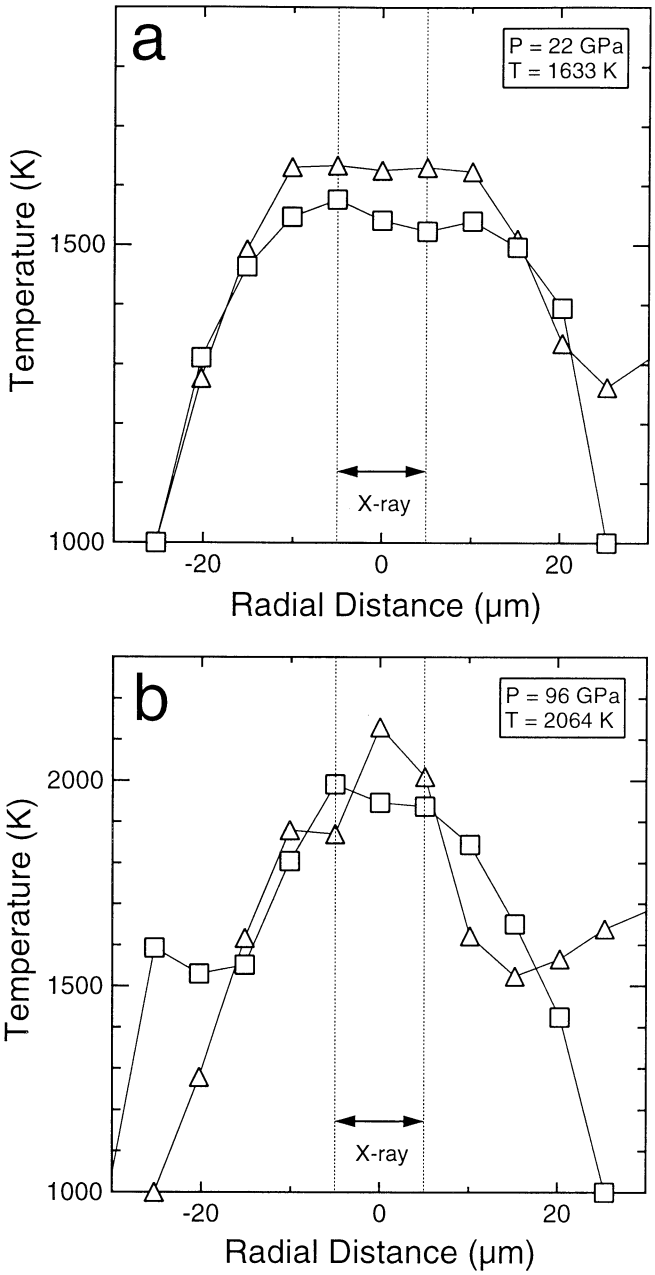

Figure 5. Temperature profiles for the heated area at (a) 22 GPa and (b) 92 GPa. To simplify the diagram, we present binned data for every third point. The two sides of the sample are denoted with different symbols. The X-ray probed area is denoted by dotted lines.

The temperature is determined by fitting the measured spectrum of thermal radiation, which is corrected for system response, to the Planck equation. Assuming gray body radiation, we fit emissivity and temperature. By measuring temperature across the heated area on both sides of the sample we obtain information on the three-dimensional temperature distribution within the X-rayed volume. To obtain the temperature of the sam-

pled volume, we assume that the temperature profile is axially symmetric, based on the observation of a heated area with an axially symmetric intensity distribution. We obtain an average temperature of the X-rayed area by integrating along the radial temperature distribution. The temperature near the edge of the probed area will contribute more to the average temperature of the sample due to its larger area. To account for this effect, we calculate the average temperature T_{avg}:

$$T_{\text{avg}} = \frac{\sum_i \int_{r_i}^{r_{i+1}} T(r)\pi r dr}{\pi R^2}, \tag{3}$$

where r is the distance from the center of heated area, $T(r)$ is the temperature at r, and R is the radius of X-ray probed area. The subscript i denotes each temperature datum along the radial direction. This is identical to taking a weighted average, and thus the estimated temperature error can be calculated using the standard deviation. The estimated error from the Planck equation fitting is also included in the calculation of error. More detailed information can be found elsewhere (A. Kavner et al., manuscript in preparation, 2000).

Since we measure the temperature profile on both sides, we directly calculate the thermal gradient along the stress axis of the DAC. To obtain the temperature for the probed volume, the temperatures from both sides are averaged. We typically heat the sample for 3 min or more while collecting a single XRD spectrum. During this time, at least three pairs of thermal radiation spectra are collected. These were used to detect time-dependent temperature fluctuations during the XRD measurement.

Including all sources of uncertainty, the estimated random error in sample temperature, $\sigma(T_{\text{sample}})$, was calculated from

$$\sigma(T_{\text{sample}})^2 = \frac{1}{2^2}\sum_{i=1}^{2}\sigma[T_i]^2 + \sigma[T_1, T_2]^2 + \frac{1}{2^2}\sum_{i=1}^{2}\sigma[T_i(t)]^2, \tag{4}$$

where σ is the estimated error, T is temperature, and $T(t)$ is the time variation of temperature. The subscript i denotes the two sides of the sample. In (4), the first term includes the error from radial thermal gradient for each side of the sample, the second term is the error from the axial thermal gradient, and the third term is the error from time variation of temperature on each side. This treatment is expected to give more reliable average temperature than simply taking the peak temperature, which has often been used in previous studies.

We used thermal radiation measured over the range 670–830 nm to fit the Planck equation. If we fit a different wavelength range (for example, dividing the range into halves or quarters and perform separate fits), the temperature difference does not exceed 20 K. The measured thermal radiation spectrum also contains some noise due to the dielectric coating of the laser optics. The error produced by this noise was determined by taking upper and lower bounds on slopes which define the noise envelope. This also contributes <20 K to the temperature uncertainty.

The radial thermal gradient has long been a significant problem in laser heating. Our approach is to improve temperature homogeneity by both decreasing the X-ray beam size and increasing the heated area. The former can be readily achieved with a third generation synchrotron source, and the latter is achieved by using a higher-mode laser beam, e.g., TEM_{01} [*Shen et al.,* 2000].

The radial gradient is still a major problem if there is misalignment between the heated area and X-ray probe area. For example, a 20-μm misalignment could result in 200 K uncertainty (see Figure 5). Furthermore, inhomogeneous distribution of absorption material could result in a situation where only part of the sample couples to the laser. In this case, the XRD pattern is obtained from material at a range of temperatures. By using submicron-sized platinum we can make a very homogeneous mixture and so minimize this problem.

The axial thermal gradient is another important error source. While decreasing the sample thickness may help to reduce this problem, this results in a poorer X-ray diffraction pattern. When single-sided heating is used and temperature is measured from both sides of the sample, the maximum axial thermal gradient was 200 K or more [*Shen et al.,* 2000]. If an insulation material is not used and the sample directly touches the diamond anvils, the axial temperature problem may be even more severe due to high thermal conductivity of diamond. Systematic error due to the axial gradient in single-sided heating can lead to overestimation of higher-order thermoelastic terms in the P–V–T EOS fit [*Shim and Duffy,* 2000].

In order to obtain a high-quality XRD pattern the sample must be heated for a sufficient period of time (typically a few minutes). The temperature should not change very much during this interval. For most of our runs, the temperature fluctuation over the data collection time was <50 K.

As a further test, we performed two different temperature profile calculations and compared these for each temperature measurement. The first is calculated by fitting the data to Planck equation as described above. In the second case, we use the following relationship between radiation intensity I and temperature for blackbody radiation:

$$I = \varepsilon\sigma T^4, \tag{5}$$

where ε is the total emissivity and σ is the Stefan-Boltzmann constant. Using the peak temperature obtained from the Planck fit and the measured intensity at the central peak temperature, we calculate the proportionality factor. Assuming that this factor is con-

stant, we then use the measured intensity to calculate temperature away from the hot spot (A. Kavner et al., manuscript in preparation, 2000). For data analysis we selected only those data points for which there is no significant difference between the temperature profile calculated by this method and the temperature profile obtained by fitting to the Planck equation.

The importance of the thermal pressure effect in LH-DAC has been extensively discussed [*Heinz,* 1990; *Fiquet et al.,* 1996; *Dewaele et al.,* 1998; *Andrault et al.,* 1998]. We account for changes in pressure during heating by measuring the diffraction line of an internal standard, platinum, at high temperature and use the P–V–T EOS of Pt [*Holmes et al.,* 1989] for pressure determination. The pressure generally changes by 5–10 GPa during heating, which shows the importance of in situ pressure measurement. While the total change in pressure during heating is typically 10–20%, we observed that the pressure may either increase or decrease during heating.

Since the pressure at elevated temperature is described by the sum of a static pressure at 300 K and thermal pressure, one needs to propagate both the temperature error and volume error into the pressure term. The estimated pressure error is

$$\sigma[P]^2 = \left(\frac{\partial P}{\partial V}\right)^2 \sigma[V(Pt)]^2 + \left(\frac{\partial P}{\partial T}\right)^2 \sigma[T]^2, \qquad (6)$$

where $\sigma[V(Pt)]$ is the estimated volume error for platinum and $\sigma(T)$ is the estimated temperature error (equation (4)).

3. Results and Discussion

3.1. Low-Pressure Phase Boundary of $CaSiO_3$ Perovskite

The phase diagram of the $CaSiO_3$ system has been studied by the LVP technique [*Wang and Weidner,* 1994; *Gasparik et al.,* 1994]. These measurements reported that the β-Ca_2SiO_4+$CaSi_2O_5$ assemblage, which is disproportionated from walstromite-type $CaSiO_3$, transforms to $CaSiO_3$ perovskite at 9–11 GPa at high temperature. In order to verify the proposed phase boundary, four heating runs covering 8–22 GPa and 300–2200 K were performed (Figure 6).

The sample was compressed without heating to 10.4 GPa, and wollastonite persists metastably to this pressure. Upon heating to 1670–1820 K, no diffraction except platinum lines was observed at high P–T. According to previous studies the P–T conditions are close to the walstromite–β-Ca_2SiO_4 + $CaSi_2O_5$ phase boundary. Walstromite [*Trojer,* 1969], β-Ca_2SiO_4 [*Jost et al.,* 1977], and $CaSi_2O_5$ [*Angel et al.,* 1996] have low symmetry (triclinic, monoclinic, and triclinic, respectively). The weak expected diffraction intensity due to low symmetry may be responsible for the lack of observed diffraction peaks. However, after quench, β-Ca_2SiO_4 diffraction lines were observed not only at the heated spot but also 20 μm away from the heated spot. Considering the thermal gradient (10–50 K/μm), it seems that β-Ca_2SiO_4 can form at fairly low temperature (about 1000 K). The X-ray exposure time required to detect the β-Ca_2SiO_4 peaks was 30 min. So the absence of the peak at high temperature may be caused by insufficient exposure time (i.e., 3 min).

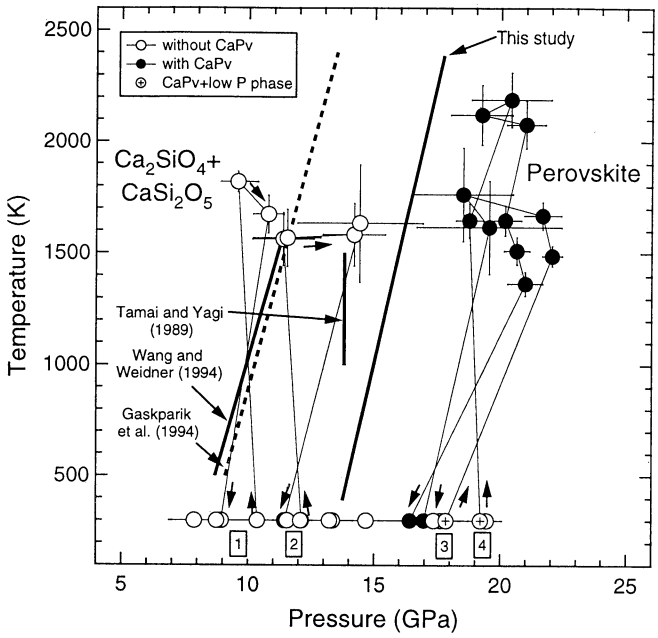

Figure 6. Phase diagram of $CaSiO_3$. The four separate heating runs are denoted with numbers. Open and solid symbols represent samples without and with $CaSiO_3$ perovskite (CaPv), respectively. The starting assemblages of $CaSiO_3$ perovskite and lower-pressure phases (this coexistence is due to incomplete transformation by short test heating) is shown by the open circle with a plus. The proposed phase boundaries between Ca_2SiO_4+$CaSi_2O_5$ and $CaSiO_3$ perovskite are plotted.

The second heating run was performed starting at 12.1 GPa. At high temperature, relatively strong diffraction lines were observed which can be identified as those of a Ca_2SiO_4 phase. Five polymorphs have been reported for this stoichiometry at ambient pressure and high temperature, i.e., γ, β, α'_L, α'_H, and α in order of increasing temperature. Although the detailed structure of some of these phases is still controversial due to their nonquenchable nature, the powder XRD patterns are well known. Using the proposed crystal structures, we calculated XRD patterns for these phases, γ [*Mumme et al.,* 1995], β [*Jost et al.,* 1977], α'_L [*Il'inets and Bikbau,* 1990], α'_H [*Mumme et al.,* 1995], and α [*Eysel and Hahn,* 1970]. The differences in the XRD patterns are very small due to the subtle differences between the structures. However, one diffraction line at 2.0 Å is strong for the high-temperature phases (α'_L and α'_H) compared to lower-temperature phases (γ and β). Indeed, in our experiment this peak is observed only

at high temperature. Furthermore, *Wang and Weidner* [1994] reported a phase transformation from β to α'_L at 9 GPa and 1350 K. Thus, this phase can be identified as the α' phase. However, the subtle difference between α'_L and α'_H prevents us from differentiating between those structures. As shown in Figure 6, this run covers P–T conditions which were reported as in the stability field of $CaSiO_3$ perovskite instead of Ca_2SiO_4 by LVP measurements.

After quench, the 2-Å line disappears but other β phase lines were observed. At 20 μm away from the heated area, we could find the peaks which can be identified as those of titanite-type $CaSi_2O_5$ [*Angel et al.,* 1996] as well as those of β-Ca_2SiO_4.

A previously unheated spot containing walstromite-type $CaSiO_3$ was found after further compression to 17.9 GPa. Before the heating run we exposed the sample to the laser for 30 s to test laser coupling and X-ray-laser alignment. Immediately after this operation, strong $CaSiO_3$ perovskite lines appeared. We performed a third heating run at this spot. At high temperature the $CaSiO_3$ perovskite diffraction lines are clearly observed. All obtained peaks are assigned to either $CaSiO_3$ perovskite or platinum. One more heating run at 19.2 GPa was performed at an area that had not been directly heated previously and which contained β-Ca_2SiO_4 peaks. Only $CaSiO_3$ perovskite and platinum peaks were observed for this run.

The P–T conditions of these observations are plotted in Figure 6. The Ca_2SiO_4+$CaSi_2O_5$ assemblage is stable to 15 GPa, and the phase boundary to $CaSiO_3$ perovskite lies between 15 and 17 GPa. In contrast, previous LVP studies reported the phase boundary at much lower pressure, 9–12 GPa. *Wang and Weidner* [1994] observed the phase boundary in situ by XRD at high P–T using LVP. They initially synthesized $CaSiO_3$ perovskite at high P–T and then decreased the pressure at a fixed temperature. The growth of the Ca_2SiO_4+$CaSi_2O_5$ assemblage at the expense of $CaSiO_3$ perovskite was used as a criterion to determine the boundary. They observed that the perovskite phase diminishes after 20 min of heating at <10 GPa and 1300 K, which means that this reaction is sluggish. Indeed, $CaSiO_3$ perovskite persists down to 1 GPa at 300 K. Although the metastable persistence will be weaker at high temperature, *Wang and Weidner*'s [1994] observation may indicate that their temperature was too low ($T < 1600$ K) to overcome the energy barrier from $CaSiO_3$ perovskite to the Ca_2SiO_4+$CaSi_2O_5$ assemblage, so that $CaSiO_3$ perovskite may be able to survive metastably in the Ca_2SiO_4+$CaSi_2O_5$ stability field in their experiment. Thus their boundary should be considered as a lower bound.

A quench experiment using the LVP was performed by *Gasparik et al.* [1994]. As shown in Figure 6, their phase boundary is similar to that of *Wang and Weidner* [1994] but 4–5 GPa lower than this study. The reason for the discrepancy with this study is not clear, but we would like to stress that our observation is based on in situ XRD measurements.

Kanzaki et al. [1991] reported the P–T conditions of the synthesis of various calcium silicate phases using the LVP. A glass was observed after quench from 15 GPa and 1800 K, which they identified as a quench product of $CaSiO_3$ perovskite. Using the LHDAC, *Tamai and Yagi* [1989] synthesized $CaSiO_3$ perovskite at $P > 13.8$ GPa, suggesting a boundary that is intermediate between this and other studies.

Although we do not have a P–T path that directly crosses the phase boundary, the high P–T data points constrain the phase boundary to within ±2 GPa. In contrast to the previous LVP study, our result is based on observation during pressure increase. Thus, the kinetics of the transformation from $CaSiO_3$ perovskite to Ca_2SiO_4+$CaSi_2O_5$ cannot affect our observation. The nature of the transformation from Ca_2SiO_4+$CaSi_2O_5$ to $CaSiO_3$ perovskite is not well known. However, in runs 3 and 4 where we start from the low-pressure phase assemblage, rapid transformation from Ca_2SiO_4+$CaSi_2O_5$ to $CaSiO_3$ perovskite was observed. So it is likely that this transformation may be less affected by kinetic effects. Strictly speaking, however, the phase boundary determined by this study is an upper bound.

3.2. Stability of $CaSiO_3$ Perovskite at Lower Mantle Conditions

The stability of $CaSiO_3$ perovskite has been confirmed to lower mantle pressures at 300 K [*Tamai and Yagi,* 1989; *Yagi et al.,* 1989; *Tarrida and Richet,* 1989; *Mao et al.,* 1989; *Shim et al.,* 2000]. However, the stability has never been studied directly at lower mantle P–T conditions. We measured the XRD patterns at in situ lower mantle conditions ($18 < P < 96$ GPa, $1238 < T < 2419$ K, Figure 1). $CaSiO_3$ perovskite diffraction lines were readily observed in all of our runs (Figure 2). No peak splitting or new peaks were found. This indicates that $CaSiO_3$ perovskite is stable to 2300 km depth in the Earth's interior.

Stixrude et al. [1996] proposed a tetragonal distortion of $CaSiO_3$ perovskite over the entire mantle pressure range at the ground state based on first principles calculations. The fact that the expected peak splitting from the distortion has never been reported at lower mantle pressures at 300 K was attributed to the low resolution of the energy dispersive X-ray diffraction (EDXD) technique. On the basis of the assumption that $CaSiO_3$ perovskite is tetragonally distorted at 300 K, the phase transformation to cubic is predicted to be 2200 K at 80 GPa [*Stixrude et al.,* 1996].

No evidence of distortion and hence the phase transformation to cubic was detected at 300 K in a related study [*Shim et al.,* 2000] and at high temperature by this study. However, calculated XRD patterns show that the peak splitting by the proposed distortion (0.7% change of c/a ratio at 300 K) may be very close to or

below the resolution limit of EDXD. Increasing temperature is expected to decrease this distortion [*Stixrude et al.,* 1996]. Thus, although we observed a 20–30% decrease in peak width at high temperature, the splitting may still not be detectable if the distortion is significantly lower than at 300 K. However, the magnitude of the proposed distortion (0.7% change of c/a ratio) is smaller than the estimated volume error. Thus it is expected that, even if exists, this distortion does not affect the P–V–T EOS fitting result. Higher-resolution techniques, such as angle-dispersive X-ray diffraction, are need to further investigate the proposed distortion.

3.3. P–V–T Equation of State of $CaSiO_3$ Perovskite

P–V–T measurements for $CaSiO_3$ perovskite have only been carried out below 12 GPa [*Wang et al.,* 1996] where the material is metastable. A long extrapolation is thus required to apply the results to the lower mantle. Furthermore, the limited P–T coverage precludes constraints on higher-order thermoelastic parameters. In this study, we used P,V,T data points at 20–69 GPa and 1272–2380 K.

According to Mie-Grüneisen theory the total pressure $P_{\rm tot}(V,T)$ at a given volume and temperature can be expressed as a sum of static compression at a reference temperature $P_{\rm st}(V,T_0)$ and the thermal pressure $\Delta P_{\rm th}$ to the temperature T at a given volume V:

$$P_{\rm tot}(V,T) = P_{\rm st}(V,T_0) + \Delta P_{\rm th}(V,T). \quad (7)$$

For the static pressure term the Birch-Murnaghan equation is used.

The Debye model can be used to describe thermal pressure term in (7). Indeed, it has been suggested that the Debye model is a good approximation for $MgSiO_3$ perovskite and MgO [*Anderson,* 1998]. We expect that the Debye assumption should be reasonable for $CaSiO_3$ perovskite as it has high symmetry and a close-packed structure. With this model, the terms in (7) are

$$P_{\rm st}(V,T_0) = \frac{3}{2}K_{T0}\left[\left(\frac{V_0}{V}\right)^{7/3} - \left(\frac{V_0}{V}\right)^{5/3}\right] \cdot \left\{1 - \frac{3}{4}(4 - K'_{T0})\left[\left(\frac{V_0}{V}\right)^{2/3} - 1\right]\right\} \quad (8)$$

$$\Delta P_{\rm th} = \frac{\gamma(V)}{V}\left[E_{\rm th}(V,T) - E_{\rm th}(V,T_0)\right], \quad (9)$$

where K_{T0} is the isothermal bulk modulus, K'_{T0} is its pressure derivative, and γ is the Grüneisen parameter. The subscript zero denotes ambient conditions. The vibrational energy can be calculated from the Debye model,

$$E_{\rm th} = \frac{9nRT}{(\theta/T)^3}\int_0^{\theta/T}\frac{\xi^3 d\xi}{e^\xi - 1}. \quad (10)$$

The Debye temperature is given by θ, n is the number of atoms in a formula unit, and the R is the gas constant. The Grüneisen parameter is assumed to be a function of volume only:

$$\gamma = \gamma_0\left(\frac{V}{V_0}\right)^q, \quad (11)$$

where q is assumed to be constant. The Debye temperature can also be described as a function of volume:

$$\theta = \theta_0 \exp\left(\frac{\gamma_0 - \gamma(V)}{q}\right). \quad (12)$$

In this approach, the fitted parameters are V_0, K_{T0}, K'_{T0}, γ_0, q, and θ_0.

This EOS has the advantage that it yields higher-order thermoelastic terms in an internally consistent way [*Stixrude and Bulkowinski,* 1990; *Jackson and Rigden,* 1996]. The first three terms (V_0,K_{T0},K'_{T0}) are obtained from 300 K data. It has been shown that q cannot be well-constrained with LVP data alone [*Jackson and Rigden,* 1996]. *Shim and Duffy* [2000] found that the increased P–T range of DAC data allows q to be better constrained. The EOS is not sensitive to the choice of θ_0.

Since the thermal gradients are the major source of error, we use only data points which have average temperatures from equation (4) with an estimated standard deviation of <150 K. These data points are listed in Table 1. Including data points with greater temperature variation does not systematically affect the result, but it increases the residual of the fit. Although the P–V–T measurements were performed to 96 GPa at high temperature, since the platinum peaks were overlapped by argon diffraction lines near megabar pressures, the calculated pressures have large uncertainties. Although we do not use these points in the fit, they are consistent with lower P–T data points.

Since $CaSiO_3$ perovskite is unstable at ambient P–T conditions, there is no direct measurement of V_0 and no elasticity measurements at ambient conditions. DAC measurements have been performed to 130 GPa at 300 K [*Tamai and Yagi,* 1989; *Yagi et al.,* 1989; *Tarrida and Richet,* 1989; *Mao et al.,* 1989]. Fitting these data to (8) yields K_{T0} = 280 GPa, assuming K'_{T0} = 4. However, LVP measurements [*Wang et al.,* 1996], systematics in the $CaTiO_3$-$CaSiO_3$ system [*Sinelnikov et al.,* 1998], and first principle calculations [*Karki and Crain,* 1998] all suggest that the bulk modulus may be smaller (230–245 GPa). Indeed, *Shim et al.* [2000] found that the previous DAC measurements are significantly contaminated by nonhydrostatic stress, so that they yield higher K_{T0}. By monitoring the *St* value, *Shim et al.* [2000] was able to characterize the stress condition of sample at high pressure. Their static compression result is used in this study (Table 2).

The Debye temperature θ_0 is normally constrained by calorimetric measurements. However, owing to the instability of $CaSiO_3$ perovskite at ambient conditions, this quantity has not been measured. For $MgSiO_3$ per-

Table 1. $CaSiO_3$ Data Used in P–V–T EOS Fitting[a]

Experiment 1, NaCl			Experiments 2–4, Ar		
P, GPa	V, Å^3	T, K	P, GPa	V, Å^3	T, K
35.5(7)	41.599(62)	1416(54)	24.3(12)	43.311(13)	1808(141)
35.2(7)	41.648(29)	1410(54)	25.0(10)	43.287(29)	1756(144)
35.5(8)	41.658(36)	1450(60)	24.6(9)	43.447(30)	1788(89)
35.9(7)	41.785(17)	1592(44)	23.6(6)	43.408(25)	1686(59)
34.8(7)	41.855(22)	1733(49)	21.9(16)	43.418(74)	1555(117)
34.8(7)	41.919(21)	1687(51)	22.4(7)	43.434(48)	1633(78)
36.1(8)	41.813(40)	1648(41)	21.6(8)	43.467(37)	1539(80)
35.4(9)	41.789(43)	1640(41)	67.4(24)	38.261(57)	1652(24)
35.8(7)	41.843(8)	1625(55)	68.4(23)	38.203(25)	1533(40)
42.8(10)	40.965(43)	1669(31)	68.5(24)	38.168(25)	1410(17)
43.4(9)	41.010(34)	1785(66)	67.2(23)	38.058(60)	1272(28)
42.3(10)	41.096(97)	1993(73)	22.0(4)	43.658(64)	1488(45)
46.6(11)	40.438(39)	1485(46)	21.7(7)	43.662(14)	1668(62)
46.3(21)	40.338(60)	1589(35)	20.6(5)	43.543(9)	1511(62)
47.2(11)	40.309(71)	1493(51)	21.0(7)	43.569(33)	1365(54)
47.4(11)	40.396(94)	1520(45)	56.2(16)	39.992(67)	2380(67)
47.2(12)	40.431(58)	1585(50)	64.3(20)	38.515(83)	1752(116)

[a]The number in parentheses is the estimated uncertainty (1σ).

ovskite it has been measured to be 1000 K [*Akaogi and Ito,* 1993]. We assume here that θ_0 of $CaSiO_3$ perovskite is the same as for $MgSiO_3$ perovskite.

By fixing V_0, K_{T0}, K'_{T0}, and θ_0, only two parameters, γ_0 and q, are fit using the Birch-Murnaghan-Debye (BMD) equation (equation (7)–(12)) and data shown in Table 1. No weighting was used. As shown in previous simulations of P–V–T data [*Shim and Duffy,* 2000], γ_0 is mainly constrained by low-pressure and high-temperature data points and q by high-pressure and high-temperature data points. For this reason, we combined our data with the LVP data [*Wang et al.,* 1996]. The fit for the combined data set yields $\gamma_0 = 1.92 \pm 0.05$ and $q = 0.6 \pm 0.3$. This result is projected on to the P–T plane is in Figure 7. The residual of fit is also shown in Figure 8. Since the residual is randomly distributed around zero, it is likely that terms of higher order than q, such as volume dependence of q itself, are not resolvable by this study.

Table 2 compares the EOS parameters from the study with those of *Wang et al.* [1996] and results for $MgSiO_3$ perovskite [*Jackson and Rigden,* 1996; *Fiquet et al.,* 2000]. The fits to the BMD equation were also performed for the individual data sets. The LVP data [*Wang et al.,* 1996] alone yields $\gamma_0 = 1.74 \pm 0.17$ and $q = -3.5 \pm 4.9$. Here γ_0 is marginally consistent with

Table 2. Thermoelastic Parameters for $CaSiO_3$ Perovskite[a]

Parameter	$CaSiO_3$ Perovskite		$MgSiO_3$ Perovskite	
	This Study	Wang	Jackson	Fiquet
V_0, cm^3 mol^{-1}	27.45(2)	27.45(2)	24.43	24.43
K_{T0}, GPa	236(4)	232(8)	262	259.5(9)
K'_{T0}	3.9(2)	4.8(3)	4.0[b]	3.69(4)
γ_0	1.92(5)	1.7[c]	1.33	1.4[c]
q	0.6(3)	1.0[b]	1.0[b]	1.4(5)
θ_0, K	1000[b]	1100[b]	1000[b]	1100[b]
α_0, 10^{-5} K^{-1}	2.2(3)	3.0(5)	1.57	2.18(12)
$(dK_T/dT)_P$, GPa K^{-1}	−0.028(11)	−0.033(8)	−0.021	−0.017(2)
δ_T	5.2(21)	4.8[c]	5.2	5.6[d]

[a]The number in parentheses is the estimated uncertainty (1σ). The thermoelastic parameters for $CaSiO_3$ perovskite are from *Wang et al.* [1996] and the thermoelastic parameters for $MgSiO_3$ perovskite are from *Jackson and Rigden* [1996] and *Fiquet et al.* [2000].

[b]Assumed value.

[c]Inferred value.

[d]Derived from the parameters given by *Fiquet et al.* [2000].

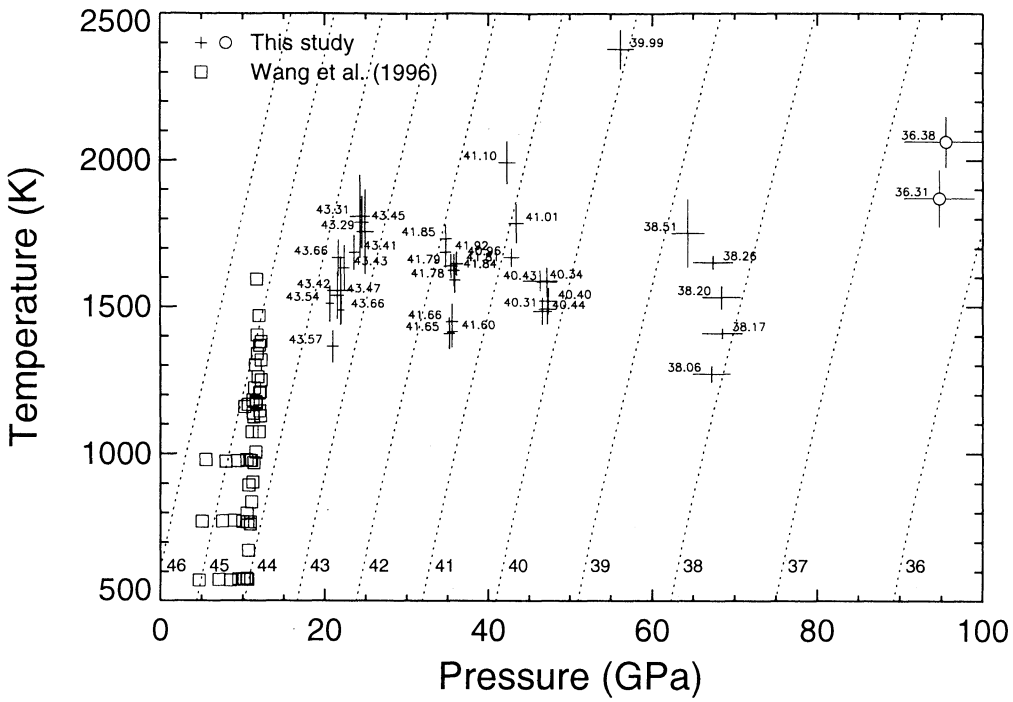

Figure 7. P–V–T data for $CaSiO_3$ perovskite projected on the P–T plane. Isochrons from the best fitting BMD equation are plotted for comparison. The measured volume of each point is listed next to the point. The error bars denote the estimated uncertainty (1σ). High-pressure data points (open circles) were not used in the fit.

the above result within the uncertainty, and q is not constrained in this case, consistent with expectations based on the simulations of *Shim and Duffy* [2000]. A fit to our P,T data points alone yields $\gamma_0 = 2.00 \pm 0.08$ and $q = 0.9 \pm 0.4$, which agrees with the above result within the uncertainty. Interestingly, the BMD fit for the LVP data set for $CaSiO_3$ perovskite does not constrain γ_0 as well as for $MgSiO_3$ perovskite data set. This is caused by the fact that the high-temperature run for $CaSiO_3$ perovskite was performed over a narrow pressure range (1–12 GPa), as shown in Figure 7, and the temperature range is smaller than that of the $MgSiO_3$ perovskite data set ($T \leq 2000$ K). Our LHDAC data for $CaSiO_3$ perovskite by itself yields a good constrain for γ_0 as well as for q.

As shown in Figure 7, the total volume variation of the LVP data is controlled by pressure and temperature by nearly equal amounts. However, it is the pressure that controls the volume variation in our data set: ~12% of the volume change is by pressure and 2% by temperature. Thus the temperature contribution is more dominant in the LVP data set than the LHDAC data set and the pressure contribution is dominant for LHDAC. In the quasi-harmonic assumption the Grüneisen parameter and its volume variation should be the same regardless of whether measured under isobaric (denoted as γ_P and q_P) or isothermal (denoted as γ_T and q_T) conditions [*Gillet et al.*, 1998]. The difference between these parameters can be attributed to anharmonic effects:

$$a = \alpha(\gamma_T - \gamma_P), \tag{13}$$

where a is the anharmonicity and α is the thermal expansivity. Assuming γ_0 from the LVP data set represents γ_{0P} and γ_0 from this data set represents γ_{0T}, the parameter a_0 can be estimated to be $0.5 \sim 0.8 \times 10^{-5}$ K^{-1}. This value is only a rough estimate, because the volume variation in the LVP data is controlled nearly equally by both pressure and temperature so a_0 may be underestimated. The a_0 value has also been measured by vibrational spectroscopy [*Gillet et al.*, 1998]. In vibrational spectroscopy the value can be measured for individual modes, but our value would be considered as a weighted average of all modes. Since the weighting scheme is not well known, it is difficult to compare our value to vibrational spectroscopy results directly. However, our value is slightly smaller than those of spectroscopy results for other mantle silicates: $0 \sim -5.9 \times 10^{-5}$ K^{-1} for β-Mg_2SiO_4 [*Reynard et al.*, 1996], $-0.5 \sim -6.0 \times 10^{-5}$ K^{-1} for forsterite [*Gillet et al.*, 1997], $0.9 \sim -2.6 \times 10^{-5}$ K^{-1} for ilmenite-type $MgSiO_3$ [*Reynard and Rubie*, 1996], and $0 \sim -10 \times 10^{-5}$ K^{-1} for $MgSiO_3$ perovskite [*Gillet et al.*, 1996]. From Raman measurements as a function of pressure and temperature, direct measurement of the anharmonic effect has been performed for $MgSiO_3$ perovskite [*Gillet et al.*, 2000]. It was also observed that the anharmonicity is small at lower mantle conditions. These observations support the use of a harmonic model for lower mantle constituents.

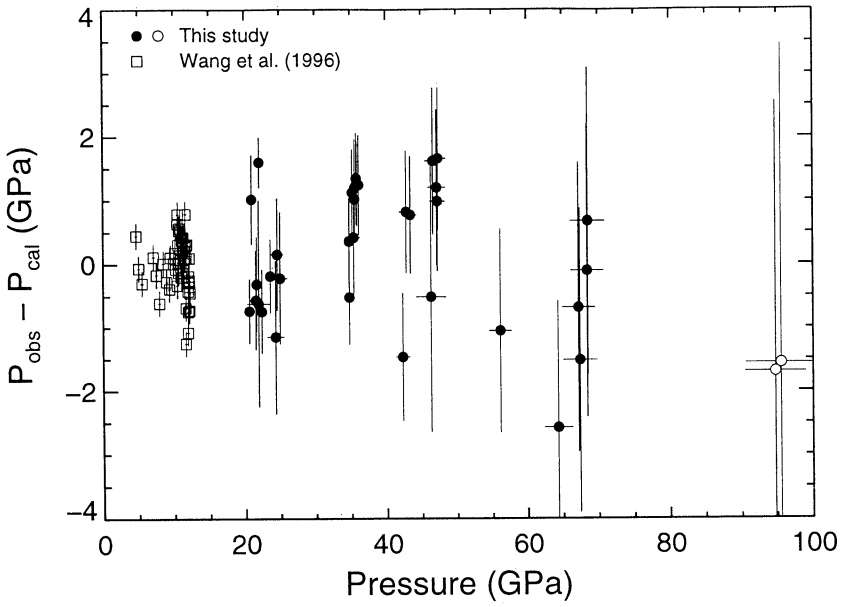

Figure 8. Residual of P–V–T EOS fit for $CaSiO_3$ perovskite. The error bars denote estimated uncertainty (1σ). Solid circles are present data used in the fitting. Open circles and squares show highest pressure data that were not used in the fitting.

We also performed a weighted fit on the combined data set using weights calculated from the estimated uncertainties for pressure, volume, and temperature. The result in this case is $\gamma_0 = 1.88 \pm 0.21$ and $q = 0.3 \pm 2.2$. As shown by *Shim and Duffy* [2000], the lower P–T measurements control the fit due to their low estimated errors for P,V,T. Thus the volume dependence term q cannot be constrained.

Above 90 GPa, we have two data points that are not used in the fitting due to the large uncertainty in measured pressure. If those are included in the combined data set, the result becomes $\gamma_0 = 1.95 \pm 0.04$ and $q = 0.9 \pm 0.2$, which yields a larger q but one that is within mutual uncertainties. Including these points expands the pressure range by 30% and hence they have a more significant effect on q than data points at lower pressure.

Earlier DAC and LVP measurements reported much different static compression curves for this material. As discussed by *Shim and Duffy* [2000], the reference static compression curve at 300 K has a strong effect on the value of q. We performed a P–V–T EOS fit for the combined data set by fixing the static compression term to that of *Wang et al.* [1996] (Table 2). As discussed above, the compression curve of earlier studies [*Tamai and Yagi,* 1989; *Yagi et al.,* 1989; *Mao et al.,* 1989; *Tarrida and Richet,* 1989] are essentially the same as that of *Wang et al.* [1996] at large compressions. A significantly different result was obtained for the fitted parameters in this case, especially for q: $\gamma = 2.06 \pm 0.05$ and $q = 2.6 \pm 0.3$. This would indicate a significant volume dependence of the thermal pressure. In this study, the data set at 300 K and high temperature were both measured under the same experimental conditions, and it was demonstrated that deviatoric stresses are minimal. Thus the results obtained by fixing the static compression term to that of *Shim et al.* [2000] are internally consistent.

Wang et al. [1996] used a high-temperature Birch-Murnaghan equation and polynomial expansion for the thermal pressure to fit their LVP data. However, the limited P–T range does not allow constraints to be placed on higher-order terms. For example, $(\partial K_T/\partial T)_P$ was not resolved directly in their EOS fit. Instead,

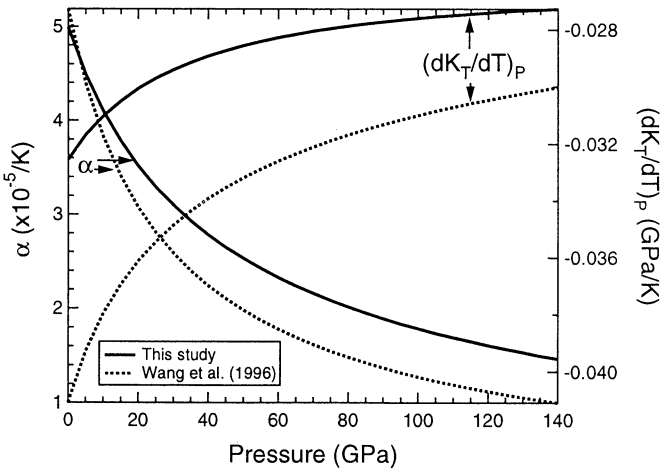

Figure 9. Thermal expansivity α and temperature dependence of bulk modulus, $(\partial K_T/\partial T)_P$, at lower mantle pressures and 2500 K. For comparison, curves calculated from the preferred parameter set by *Wang et al.* [1996] are also presented.

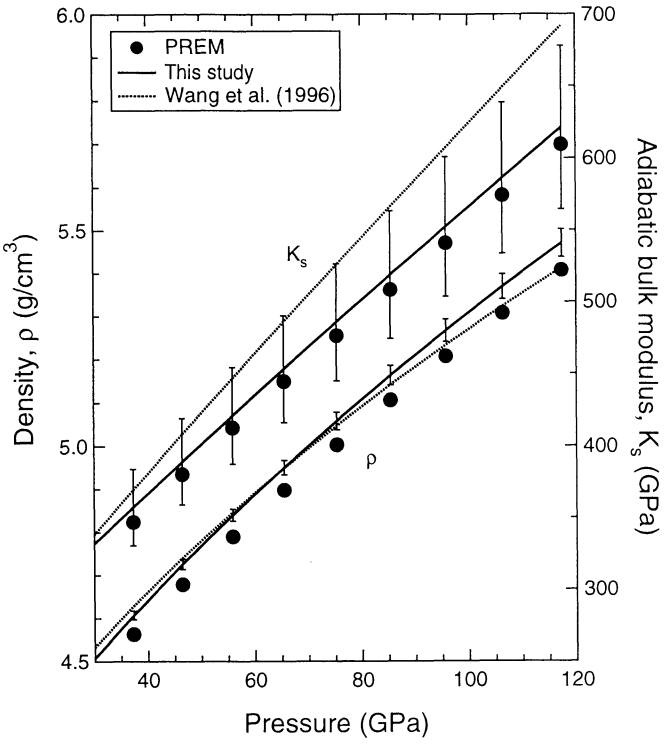

Figure 10. Density and adiabatic bulk modulus of $CaSiO_3$ perovskite at lower mantle P–T conditions calculated using the parameters of this study (solid lines) and *Wang et al.* [1996] (dotted lines) together with the BMD equation. Seismic data (PREM) are shown as solid circles. The error bars for this study denote the estimated uncertainty (1σ) calculated from Table 2.

by interpolating data points to isochoric and isobaric conditions they obtained this parameter as well as α_0. Other parameters were then derived from these. To compare with our results, we list their preferred parameters in Table 2.

Using the BMD results, α and $(dK_T/dT)_P$ were determined at 1 bar and 300 K (Table 2) and for 0–120 GPa and 2500 K (Figure 9) using the values in Table 2 and the equations given by *Jackson and Rigden* [1996].

At 1 bar and 300 K, $(\partial K_T/\partial T)_P$ is consistent for both studies, but the present α_0 is significantly lower than that of *Wang et al.* [1996]. Since $CaSiO_3$ perovskite is unstable at ambient conditions, direct measurement of α_0 is not possible. This value from both studies is basically a projection of high P–T data to ambient conditions. The calculations of α and $(\partial K_T/\partial T)_P$ at high pressure and 2500 K (Figure 9) show that our γ_0 and q yields smaller temperature sensitivity of bulk modulus and larger temperature sensitivity of density than those of *Wang et al.* [1996] at lower mantle conditions.

The thermoelastic parameters of $CaSiO_3$ perovskite are also compared with those of $MgSiO_3$ perovskite in Table 2. Unfortunately, K'_{T0} and q of $MgSiO_3$ perovskite from currently available data show significant discrepancies, 3.6–4.0 and 1.3–2.7, respectively. Here we present the result by *Jackson and Rigden* [1996], which assumes $q = 1$, and the LHDAC result by *Fiquet et al.* [2000]. Significant differences between $CaSiO_3$ perovskite and $MgSiO_3$ perovskite can be found for the bulk modulus and Grüneisen parameter.

Profiles of density ρ and adiabatic bulk modulus K_S were calculated using the BMD equation at lower mantle P–T conditions (Figure 10) and compared with the seismic model PREM [*Dziewonski and Anderson,* 1981]. Lower mantle temperatures were taken from *Brown and Shankland* [1981]. The density and adiabatic bulk modulus of $CaSiO_3$ perovskite are very close to that of the lower mantle: 3% greater for the adiabatic bulk modulus but indistinguishable within estimated error and 1.5% greater for density. However, the bulk modulus reported by *Wang et al.* [1996] is significantly higher than that of PREM (6.5–13.5%).

4. Conclusion

Recent improvements in the laser heated diamond anvil cell (LHDAC) technique open up new opportunities to measure material properties at the conditions of the deep interior of the Earth. The phase boundary between Ca_2SiO_4+$CaSi_2O_5$ and $CaSiO_3$ perovskite was found by in situ measurements to lie at 14–16 GPa in contrast to earlier large-volume press (LVP) results which reported 9–11 GPa. This work demonstrates that the LHDAC can be used for in situ determination of phase boundaries.

The stability of cubic $CaSiO_3$ perovskite was demonstrated to 2200 km depth (96 GPa). No evidence of a phase transformation such as tetragonal distortion or break down to oxides was observed. However, a very small tetragonal distortion (c/a ratio change <0.7%) would not be detectable by this work. Since the magnitude of distortion is smaller than the estimated volume error of this study, even if it exists, our EOS fit result may not be affected significantly.

In this study, energy dispersive X-ray diffraction measurements were performed directly at lower mantle P–T conditions. Data covering 20–69 GPa and 1272–2380 K as well as 16–105 GPa at 300 K were combined with data of *Wang et al.* [1996] (P =0–12 GPa, T =300–1600 K) and fit to the Birch-Murnaghan-Debye (BMD) equation. Only data showing homogeneous temperatures, small thermal gradient, and hydrostatic stress conditions were used in the fitting. The complete set of thermoelastic parameters are $V_0 = 27.45 \pm 0.02$ mol/cm^2, $K_{T0} = 236 \pm 4$ GPa, $K'_{T0} = 3.9 \pm 0.2$, $\gamma_0 = 1.92 \pm 0.05$, $q = 0.6 \pm 0.3$. Using this equation, we calculate not only the density and bulk modulus but also higher-order thermoelastic terms (e.g., $(\partial K_T/\partial T)_P$, α) at lower mantle P–T conditions (Figure 9).

In contrast to previous results, both the density and bulk modulus of $CaSiO_3$ perovskite are very close to

those of lower mantle seismic models. In an earlier mantle chemical model [*Ita and Stixrude,* 1992] a chemically distinct lower mantle was proposed. Bulk sound velocity profiles for upper mantle mineral assemblages were unable to fit the lower mantle seismic models. A major reason for this discrepancy was their choice of high bulk modulus of $CaSiO_3$ perovskite ($K_{T0} = 301.4$ GPa). Our results indicate that the bulk modulus of $CaSiO_3$ perovskite is much smaller at lower mantle conditions.

Acknowledgments. We thank S. Speziale and A. Kavner for experimental assistance and R. Boehler, G. Fiquet, and P. Gillet for valuable comments. This work was supported by the NSF. Portions of this work were performed at GeoSoilEnviroCARS (GSECARS), Sector 13, Advanced Photon Source at Argonne National Laboratory. GSECARS is supported by the National Science Foundation-Earth Sciences, Department of Energy-Geosciences, W. M. Keck Foundation, and the U.S. Department of Agriculture. Use of the Advanced Photon Source was supported by the U.S. Department of Energy, Basic Energy Sciences, Office of Energy Research, under contract W-31-109-Eng-38.

References

Akaogi, M., and E. Ito, Heat capacity of $MgSiO_3$ perovskite, *Geophys. Res. Lett., 20,* 105-108, 1993.

Anderson, O. L., Thermoelastic properties of $MgSiO_3$ perovskite using the Debye approach, *Am. Mineral., 83,* 23-35, 1998.

Andrault, D., G. Fiquet, J. P. Itie, P. Richet, P. Gillet, D. Häusermann, and M. Hanfland, Thermal pressure in the laser-heated diamond-anvil cell: An X-ray diffraction study, *Eur. J. Mineral., 10,* 931-940, 1998.

Angel, R. J., N. L. Ross, F. Seifert, and T. F. Fliervoet, Structural characterization of pentacoordinate silicon in a calcium silicate, *Nature, 384,* 441-444, 1996.

Boehler, R., Melting and thermal expansivity at high pressure: some new data, paper presented at the Third NIRIM International Symposium on Advanced Materials: New Trends in High Pressure Research, Nat. Inst. for Res. in Inorg. Mater., Tsukuba, Japan, 1996.

Boehler, R., N. von Bargen, and A. Chopelas, Thermal expansion, and phase transitions cf iron at high pressures, *J. Geophys. Res., 95,* 21,731-21,736, 1990.

Brown, J. M., and T. J. Shankland, Thermodynamic parameters in the Earth as determined from seismic profiles, *Geophys. J. R. Astron. Soc., 66,* 576-596, 1981.

Dewaele, A., G. Fiquet, and P. Gillet, Temperature and pressure distribution in the laser-heated diamond-anvil cell, *Rev. Sci. Instrum., 69,* 2421-2426, 1998.

Dewaele, A., G. Fiquet, D. Andrault, and D. Häusermann, P–V–T equation of state of periclase from synchrotron radiation measurements, *J. Geophys. Res., 105,* 2869-2877, 2000.

Duffy, T. S., and D. L. Anderson, Seismic velocities in mantle minerals and the mineralogy of the upper mantle, *J. Geophys. Res., 94,* 1895-1912, 1989.

Duffy, T. S., G. Shen, D. L. Heinz, and A. K. Singh, Lattice strains in gold and rhenium under non-hydrostatic compression to 37 GPa, *Phys. Rev. B Condens. Matter, 60,* 15,063-15,073, 1999.

Dziewonski, A. M., and D. L. Anderson, Preliminary Reference Earth Model, *Phys. Earth Planet. Inter., 25,* 297-356, 1981.

Eysel, W., and T. Hahn, Polymorphism and solid solution of Ca_2GeO_4 and Ca_2SiO_4, *Z. Kristallogr., 131,* 322-341, 1970.

Fiquet, G., D. Andrault, J. P. Itie, P. Gillet, and P. Richet, X-ray diffraction of periclase in a laser-heated diamond-anvil cell, *Phys. Earth Planet. Inter., 95,* 1-17, 1996.

Fiquet, G., D. Andrault, A. Dewaele, T. Charpin, M. Kunz, and D. Häusermann, P–V–T equation of state of $MgSiO_3$ perovskite, *Phys. Earth Planet. Inter., 105,* 21-31, 1998.

Fiquet, G., A. Dewaele, D. Andrault, M. Kunz, and T. L. Bihan, Thermoelastic properties and crystal structure of $MgSiO_3$ perovskite at lower mantle pressure and temperature conditions, *Geophys. Res. Lett., 27,* 21-24, 2000.

Gasparik, T., K. Wolf, and C. M. Smith, Experimental determination of phase relations in the $CaSiO_3$ system from 8 to 15 GPa, *Am. Mineral., 79,* 1219-1222, 1994.

Gillet, P., F. Guyot, and Y. Wang, Microscopic anharmonicity and equation of state of $MgSiO_3$-perovskite, *Geophys. Res. Lett., 23,* 3043-3046, 1996.

Gillet, P., I. Daniel, and F. Guyot, Anharmonic properties of Mg_2SiO_4-forsterite measured from the volume dependence of the Raman spectrum, *Eur. J. Mineral., 9,* 255-262, 1997.

Gillet, P., R. J. Hemley, and P. F. McMillan, Vibrational properties at high pressures and temperature, in *Ultrahigh-Pressure Mineralogy, Rev. Mineral.,* vol. 37, edited by R. J. Hemley, pp. 525-590, Mineral. Soc. of Am., Washington, D.C., 1998.

Gillet, P., I. Daniel, F. Guyot, J. Matas, and J.-C. Chervin, A thermodynamic model for $MgSiO_3$-perovskite derived from pressure, temperature and volume dependence of the Raman mode frequencies, *Phys. Earth Planet. Inter., 117,* 361-384, 2000.

Heinz, D. L, Thermal pressure in the laser-heated diamond anvil cell, *Geophys. Res. Lett., 17,* 1161-1164, 1990.

Hirose, K., Y. Fei, Y. Z. Ma, and H.-K. Mao, The fate of subducted basaltic crust in the Earth's lower mantle, *Nature, 397,* 53-56, 1999.

Holmes, N. C., J. A. Moriarty, G. R. Gathers, and W. J. Nellis, The equation of state of platinum to 660 GPa (6.6 Mbar), *J. Appl. Phys., 66,* 2962-2967, 1989.

Il'inets, A. M., and M. Y. Bikbau, Structural mechanism of polymorphic transitions of dicalcium silicate, Ca_2SiO_4, part II, Refinement of crystal structure of high-temperature α'_L modification of dicalcium silicate Ca_2SiO_4, *Sov. Phys. Crystallogr., 35,* 54-56, 1990.

Ita, J., and L. Stixrude, Petrology, elasticity and composition of the mantle transition zone, *J. Geophys. Res., 97,* 6842-6866, 1992.

Jackson, I., and S. M. Rigden, Analysis of P–V–T data: Constraints on the thermoelastic properties of high-pressure minerals, *Phys. Earth Planet. Inter., 96,* 85-112, 1996.

Jost, K. H., B. Ziemer, and R. Seydel, Redetermination of the structure of β-dicalcium silicate, *Acta Crystallogr., Sect. B Struct. Sci., 33,* 1696-1700, 1977.

Kanzaki, M., J. F. Stebbins, and X. Xue, Characterization of quenched high pressure phases in $CaSiO_3$ system by XRD and $_{29}Si$ NMR, *Geophys. Res. Lett., 18,* 463-466, 1991.

Karki, B. B. and J. Crain, First-principles determination of elastic properties of $CaSiO_3$ perovskite at lower mantle pressures, *Geophys. Res. Lett., 25,* 2741-2744, 1998.

Mao, H.-K., T. Yagi, and P. M. Bell, Mineralogy of the Earth's deep mantle: Quenching experiments on mineral compositions at high pressure and temperature, *Yearbook Carnegie Inst. Washington, 76,* 502-504, 1977.

Mao, H.-K., L. C. Chen, R. J. Hemley, A. P. Jephcoat, and Y. Wu, Stability and equation of state of $CaSiO_3$-perovskite to 134 GPa, *J. Geophys. Res., 94,* 17,889-17,894, 1989.

Mumme, W. G., R. J. Hill, G. Bushnell-Wye, and E. R. Segnit, Rietveld crystal structure refinements, crystal chem-

istry and calculated powder diffraction data for the polymorphs of dicalcium silicate and related phases, *Neues Jahrb. Mineral. Abh., 169,* 35-68, 1995.

Oguri, K., N. Funamori, F. Sakai, T. Kondo, T. Uchida, and T. Yagi, High-pressure and high-temperature phase relations in diopside $CaMgSi_2O_6$, *Phys. Earth Planet. Inter., 104,* 363-370, 1997.

Reynard, B., and D. C. Rubie, High-pressure, high-temperature Raman sepctroscopic study of ilmenite-type mgsio$_3$, *Am. Mineral., 81,* 1092-1096, 1996.

Reynard, B., F. Takir, F. Guyot, G. D. Gwanmesia, R. C. Liebermann, and P. Gillet, High-temperature Raman spectroscopic and X-ray diffraction study of β-Mg_2SiO_4: Insights into its high-temperature thermodynamic propoerties and the β- to α-phase-transformation mechanism and kinetics, *Am. Mineral., 81,* 585-594, 1996.

Ringwood, A. E., *Composition and Petrology of the Earth's Mantle,* McGraw-Hill, New York, 1975.

Rivers, M. L., T. S. Duffy, Y. Wang, P. J. Eng, S. R. Sutton, and G. Shen. A new facility for high-pressure research at the advanced photon source, in *Properties of Earth and Planetary Materials at High Pressure and Temperature,* Geophys. Monogr. Ser. vol. 101, edited by M. H. Manghnani and T. Yagi, pp. 79-87, AGU, Washington, D.C., 1998.

Shen, G., and P. Lazor, Measurement of melting temperatures of some minerals under lower mantle pressures, *J. Geophys. Res., 100,* 17699-17713, 1995.

Shen, G., H.-K. Mao, and R. J. Hemley, Laser-heated diamond anvil cell technique: double-sided heating with multimode Nd:YAG laser, paper presented at the Third NIRIM International Symposium on Advanced Materials: New Trends in High Pressure Research, Nat. Inst. for Res. in Inorg. Mater., Tsukuba, Japan, 1996.

Shen, G., H.-K. Mao, R. J. Hemley, T. S. Duffy, and M. L. Rivers, Melting and crystal structure of iron at high pressures and temperatures, *Geophys. Res. Lett., 25,* 373-377, 1998.

Shen, G., M. L. Rivers, Y. Wang, and S. R. Sutton, New developments on laser heated diamond anvil cell, *Rev. High Pressure Sci. Technol., 8,* in press, 2000.

Shim, S.-H. and T. S. Duffy, Constraints on the P–V–T equation of state of $MgSiO_3$ perovskite, *Am. Mineral., 85,* 354-363, 2000.

Shim, S.-H., T. S. Duffy, and G. Shen, P–V–T equation of state of $MgSiO_3$ and $CaSiO_3$ perovskites to 60 GPa and 2000 K, *Eos Trans. AGU, 79(45), Fall Meet. Suppl.,* F861, 1998.

Shim, S.-H., T. S. Duffy, and G. Shen, The equation of state of $CaSiO_3$ perovskite to 108 GPa at 300 K, *Phys. Earth Planet. Inter., 120,* 327-338, 2000.

Sinelnikov, Y. D., G. Chen, and R. C. Liebermann, Elasticity of $CaTiO_3$–$CaSiO_3$ perovskites, *Phys. Chem. Miner., 25,* 515-521, 1998.

Singh, A. K., The lattice strains in a specimen (cubic system) compressed nonhydrostatically in an opposed anvil device, *J. Appl. Phys., 73,* 4278-4286, 1993.

Stixrude, L., and M. S. T. Bukowinski, Fundamental thermodynamic relations and silicate melting with implications for the constitution of D", *J. Geophys. Res., 95,* 19,311-19,325, 1990.

Stixrude, L., R. E. Cohen, R. Yu, and H. Krakauer, Prediction of phase transition in $CaSiO_3$ perovskite and implications for lower mantle structure, *Am. Mineral., 81,* 1293-1296, 1996.

Tamai, H., and T. Yagi, High-pressure and high-temperature phase relations in $CaSiO_3$ and $CaMgSi_2O_6$ and elasticity of perovskite-type $CaSiO_3$, *Phys. Earth Planet. Inter., 54,* 370-377, 1989.

Tarrida, M., and P. Richet, Equation of state of $CaSiO_3$ perovskite to 96 GPa. *Geophys. Res. Lett., 16,* 1351-1354, 1989.

Trojer, F. J, The crystal structure of a high-pressure polymorph of $CaSiO_3$, *Z. Kristallogr., 130,* 185-206, 1969.

Wang, Y., and D. J. Weidner, Thermoelasticity of $CaSiO_3$ perovskite and implications for the lower mantle, *Geophys. Res. Lett., 21,* 895-898, 1994.

Wang, Y., D. J. Weidner, and F. Guyot, Thermal equation of state of $CaSiO_3$ perovskite, *J. Geophys. Res., 101,* 661-672, 1996.

Yagi, T., S. Kusanagi, Y. Tsuchida, and Y. Fukai, Isothermal compression and stability of perovskite-type $CaSiO_3$, *Proc. Jpn. Acad., Ser. B-Phys., 65,* 129-132, 1989.

Zerr, A., G. Serghiou, and R. Boehler, Melting of $CaSiO_3$ perovskite to 430 kbar and first in-situ measurements of lower mantle eutectic temperatures, *Geophys. Res. Lett., 24,* 909-912, 1997.

T. S. Duffy and S.-H. Shim Department of Geosciences, Princeton University, Guyot Hall, Washington Road, Princeton, NJ 08544. (e-mail: sangshim@princeton.edu; duffy@princeton.edu)

G. Shen, GSECARS, University of Chicago, Chicago, IL 60637 (e-mail: shen@cars1.uchicago.edu)

(Received December 14, 1999; revised May 3, 2000; accepted May 22, 2000.)